International Journal of Technology
http://ijtech.eng.ui.ac.id

Research Article

Venturi Flotation Column Design for Selective Recovery of Pb and Zn from Fe Using Corn Starch under Controlled pH Conditions

Reza Miftahul Ulum[1*], **Syahrul Ananta**[1], **Defranata Harianja**[1]

[1]Department of Metallurgical and Materials Engineering, Faculty of Engineering, University of Indonesia, Kampus Baru UI, Depok, 16424, Indonesia

[*]Corresponding author: reza.ulum@ui.ac.id; Tel.: +622178888111

Abstract: Froth flotation is a key technique for the selective beneficiation of sulfide ores, particularly in separating galena (PbS) and sphalerite (ZnS) from pyrite (FeS_2). However, conventional depressants such as sodium cyanide pose environmental and safety concerns. In this study, we investigated the use of corn starch as a biodegradable depressant in combination with an improved-designed Venturi-type flotation column to enhance the selective separation of lead and zinc from pyrite. A synthetic mixture of a raw material was prepared for flotation experiments under varying pH conditions (4, 7, and 10) and corn starch concentrations (0, 12.5, and 25 ppm). The Venturi column was optimized using computational fluid dynamics simulations and experimental trials, with the optimal air flow rate identified as 5 L/min for generating stable bubbles and enhancing bubble–particle interactions. Results showed that corn starch selectively depressed pyrite without significantly affecting galena floatability, particularly under alkaline conditions. The highest selectivity, indicated by a 43.62% Pb–Fe recovery gap, was achieved at pH 10 with 12.5 ppm starch. Sphalerite exhibited moderate sensitivity to starch dosage, with the best Zn–Fe separation observed at pH 4. XRF and XRD analyses confirmed the effective mineral separation, and the Pourbaix diagrams explained the electrochemical basis of the observed trends. This approach provides a sustainable and efficient alternative to conventional flotation.

Keywords: Corn starch; Flotation; Galena; Pyrite; Sphalerite

1. Introduction

Froth flotation has long been established as a vital technique in the beneficiation of sulfide ores, particularly for the recovery of valuable metals such as lead and zinc from their respective sulfide minerals galena (PbS) and sphalerite (ZnS) (Nayak et al., 2022). One of the major challenges in processing these ores is their separation from iron-bearing sulfides such as pyrite (FeS_2), whose surface chemistry and floatability often overlap with the target minerals. Achieving selective separation remains crucial for maximizing metal recovery and improving the efficiency of downstream metallurgical operations. Froth flotation is a mineral processing method used to reduce impurities before metallurgy extraction operations. Various extraction metallurgy operations, such as hydrometallurgy, pyrometallurgy, electrometallurgy, or a combination of these methods, can be implemented to further reduce impurity levels (Prameswara et al., 2023; Tjhia et al., 2024; Trisnawati et al., 2020).

Traditionally, the selective depression of unwanted minerals, such as pyrite, relies heavily on inorganic depressants, such as sodium cyanide and sodium dichromate (Nagaraj & Farinato, 2016; Prasad, 1992). These reagents can effectively alter surface hydrophobicity and electrochemical properties, allowing collectors to selectively adsorb onto target minerals. However, their high toxicity and environmental persistence have raised significant ecological and safety concerns, prompting regulatory restrictions and a search for more sustainable alternatives.

https://doi.org/10.14716/ijtech.v17i4.8368
Received July 2025; Revised February 2026; Accepted April 2026

In recent years, natural polymers, particularly polysaccharides, have garnered attention as environmentally friendly flotation reagents (Asimi-Neisiani et al., 2023; Wang, 2002). Polymers, such as dextrin, guar gum, and corn starch, exhibit nontoxic, biodegradable properties and have demonstrated promising selective depressant behavior (Qin et al., 2013; Zhao et al., 2025). These polysaccharides interact with sulfide mineral surfaces through various mechanisms, including electrostatic attraction, hydrogen bonding, and complexation with surface hydroxides (Mu et al., 2016). Corn starch can depress pyrite without significantly affecting the floatability of galena and sphalerite, especially when the pH is carefully controlled to favor selective adsorption.

Advances in flotation reactor design have introduced alternatives to conventional mechanically agitated cells, which often produce coarse bubbles and consume high energy. One such innovation is the Venturi-type flotation column, which uses hydrodynamic cavitation to generate microbubbles without mechanical agitation (Li, 2022; Li et al., 2018). This method improves recovery while reducing energy consumption (Zhou et al., 2020).

This study presents an integrated approach to sustainable mineral processing that combines the use of corn starch as a biodegradable depressant with the design and application of a Venturi-type flotation column for the selective separation of lead and zinc from iron sulfides. The research aims to enhance flotation efficiency while reducing chemical toxicity and energy consumption by addressing both environmental and technical challenges. Flotation experiments were conducted using a mixed mineral system of galena, sphalerite, and pyrite, with controlled pH (4, 7, and 10) and corn starch dosage (0, 12.5, and 25 ppm). This approach seeks to bridge current gaps in flotation selectivity and reagent sustainability by investigating the interactions between biopolymers and mineral surfaces under varying chemical conditions. The findings of this study are expected to provide valuable insights into the mechanisms of mineral selectivity and biopolymer adsorption, offering a practical, eco-friendly alternative for future flotation practices in the mining industry.

2. Methods

2.1 Materials

The flotation tests were performed using a synthetic mixture of galena (PbS), sphalerite (ZnS), and pyrite (FeS_2). Minerals were collected from natural deposits in West Java, Indonesia, and selected based on their high purity (≥99%). XRF analysis revealed a dominance of lead (Pb), zinc (Zn), and iron (Fe) elements (Table 1), while XRD confirmed the presence of corresponding sulfide compounds (Figure 1). The samples were manually crushed and ground using a laboratory-scale mini ball mill and then sieved using a sieve shaker to obtain a particle size finer than -44 μm (P80), ensuring compatibility with fine-particle flotation. Corn starch (Sigma-Aldrich, analytical grade, ≥99% purity) was used as a biodegradable depressant because of its eco-friendliness and selective adsorption properties. The collector used was potassium amyl xanthate (PAX; Merck, ≥90%), known for strong chemisorption on sulfide surfaces through thiol groups. Pine oil (Merck, reagent grade) was used as the frother due to its stable froth-forming characteristics. All flotation reagents were prepared in freshly deionized water (pH 7, resistivity >18 MΩ·cm). The pH of the slurry is controlled with NaOH or HCl solutions. The construction of the column test design used in this study was adapted from a previous study ((Xiong & Peng, 2015)), with some design parts being modified.

Table 1 XRF characterization of the initial ore sample

Element	Pb	S	Fe	Zn	Si	Mg
Concentration (%)	6.27	38.25	32.10	15.64	3.60	2.85

An improved Venturi flotation column was fabricated using transparent acrylic with an internal diameter of 4 cm and a total height of 100 cm. The system consisted of three key zones: (1) the collection zone at the lower section, (2) the froth zone 30 cm above the column top, and

(3) a foam launder for concentrate collection. The column was equipped with two inlet ports: one from the top for slurry feeding and one from the bottom for bubble generation via a Venturi tube. Based on Bernoulli's principle, the Venturi tube used in this system was self-assembled and modified at the jet-nozzle inlet to improve the pressure differential and enhance bubble formation. The detailed 2D geometry was designed using SolidWorks CAD software, which incorporates a symmetrical converging–diverging flow channel. Table 2 lists the dimensional specifications of the Venturi component.

Table 2 The dimensional specifications of the Venturi component

No.	Component	Dimension
1	Inlet diameter	1.5 cm
2	Inlet angle	27°
3	Throat diameter	0.375 cm
4	Throat length	1.125 cm
5	Outlet angle	12°
6	Outlet diameter	1.5 cm

To monitor and control fluid dynamics, the system was equipped with five YF-B1 flow sensors (1–25 L/min), responsible for tracking airflow, slurry feed, and wash water injection in real time. Data from these sensors were processed by an Arduino UNO R3 (ATmega328P) microcontroller, which simultaneously displayed individual readings on five I^2C 16×2 LCD modules. Additionally, four relay modules were integrated to automate pump operation timing according to the programmed flotation sequence. The control circuit was fully programmed and compiled using Arduino IDE, enabling synchronized automation and real-time monitoring of the flotation process.

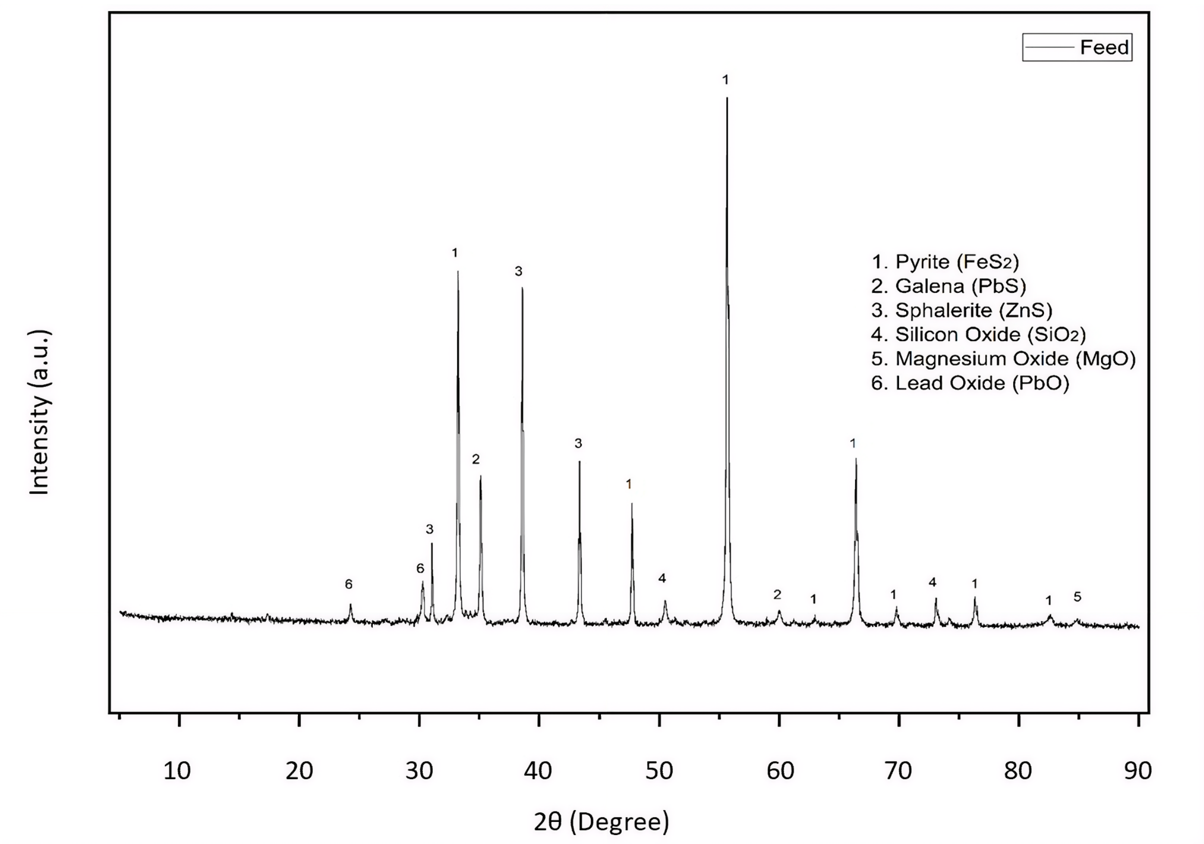

Figure 1 XRD characterization of the feed which consist of the synthetic mixture of galena, sphalerite, and pyrite

2.2 Methods

2.2.1 Preliminary Optimization of the System

Before flotation testing, the performance of the Venturi-based flotation column was evaluated and optimized to ensure efficient microbubble generation. The optimization focused on varying the injected air flow rates (4, 5, and 6 L/min) and observing the resulting bubble characteristics, including size, stability, and retention time (Table 3). These parameters were critical in establishing the optimal hydrodynamic conditions for selective flotation. Computational Fluid Dynamics (CFD) simulations were conducted as a preliminary step to visualize the fluid flow behavior and bubble formation within the modified Venturi system (Sakamatapan et al., 2021). The simulation helped confirm the pressure drop, velocity profile, and air–liquid mixing efficiency in the improved Venturi geometry prior to physical testing (Zhou et al., 2025; Wills and Finch, 2016). Table 4 shows the process variables selected for galena flotation used in this study.

Table 3 Operational variables for the froth flotation column system

Variable	Description
Independent	Airflow rate into the venturi (4, 5, and 6 L/min)
Controlled	Slurry feed: 4 L/min, internal loop: 3 L/min, and wash water: 0.3 L/min
Dependent	Bubble size, stability, and retention time

Table 4 Process variables for the flotation of Galena

Variable	Description
Independent	Slurry pH levels: 4 (acidic), 7 (neutral), and 10 (alkaline); concentrations of corn starch depressants: 0, 12.5, and 25 ppm
Controlled	Galena particle size <44 μm; slurry solid content 4%; collector (PAX) 150 ppm; frother (pine oil) 150 ppm; corn starch depressant; deionized water; pH adjusted using NaOH or HCl
Dependent	Lead (Pb) recovery (%) from Galena as the primary indicator of flotation performance

2.2.2 Flotation Setup and Procedure

The flotation experiments were conducted using galena ore to investigate the effect of slurry pH and depressant concentration on lead recovery. Initially, 80 g of the galena sample was subjected to ultrasonic agitation for 15 min to remove surface impurities and ensure uniform particle dispersion. The cleaned ore was then mixed with deionized water (1.92 L) to form a slurry with 4% solid content. The slurry was conditioned in four sequential steps over a total of 15 min: pH adjustment using either NaOH or HCl (5 min), addition of corn starch as a depressant at concentrations of 0, 12.5, or 25 ppm (5 min), introduction of potassium amyl xanthate (PAX) collector at a fixed concentration of 150 ppm (3 min), and finally, addition of pine oil as a frother at 150 ppm (2 min). The conditioned slurry was then transferred into a custom-built 2-m-high Venturi flotation column, where flotation was performed for 10 min. The Venturi system generated fine bubbles to enhance particle–bubble interactions, while air was supplied at a fixed rate of 5 L/min. Slurry and wash water flow rates were monitored and controlled in real time using flow sensors connected to a microcontroller system. Upon completion of flotation, the froth product (concentrate) and residual slurry (tailings) were collected, oven-dried at 200 °C for 3 h, and weighed to determine the metal recovery efficiency.

2.2.3 Analytical Methods and Calculation of Recovery

The elemental compositions of the feed, concentrate, and tailings were analyzed using X-ray fluorescence (XRF) to quantify the Pb, Zn, and Fe contents. Additionally, X-ray diffraction (XRD) analysis was performed on selected samples to identify mineralogical phases and validate the selective separation effectiveness. The percentage recovery of Pb was calculated using Equation 1 (Wills and Finch, 2016):

$$\text{Recovery}(\%) = \frac{C \cdot f}{F \cdot c} \times 100\% \tag{1}$$

where:

C = mass of concentrate (g)

f = Pb/Zn/Fe grade in the concentrate (%)

F = feed mass (g)

c = Pb/Zn/Fe grade in the feed (%)

The same equation was used to determine the recovery of Zn and Fe for comparative analysis. The difference in recovery percentage between the target metal (Pb or Zn) and Fe was used as a key indicator of flotation selectivity. A higher recovery gap indicates a more effective pyrite depression.

3. Results and Discussion

3.1 Result

3.1.1 Simulation Analysis and Air Flow Rate Trials of the Venturi System

CFD simulations were conducted in SolidWorks Flow Simulation 2023 using the experimental Venturi geometry. Air was modeled as the working fluid, solving the incompressible RANS Navier–Stokes equations with a k–ε turbulence model under inlet flow rates of 4–7 L·min^{-1} and a 0 Pa outlet. A Cartesian mesh with refinement ensured mesh independence (<2% ΔP variation), yielding reliable velocity and pressure distributions for comparison with experiments. At 4 L/min, the flow remained stable and well directed but was insufficient to generate a uniform distribution of fine bubbles. At 5 L/min, the lowest pressure was achieved precisely at the throat without inducing flow reversal or turbulence, indicating optimal operating conditions. At 6 L/min, the increased pressure led to flow instability characterized by turbulence and signs of cavitation risk. The velocity profiles are shown in Figure 2.

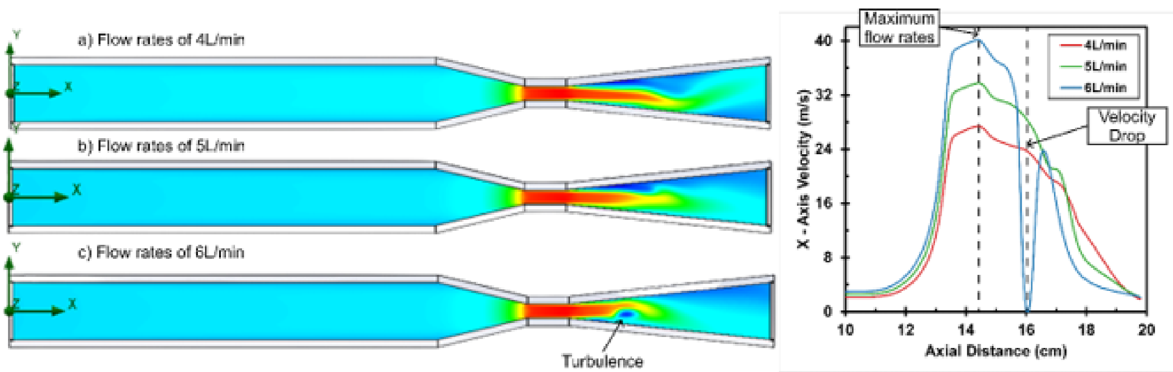

Figure 2 CFD velocity profiles at airflow rates of 4, 5, and 6 L/min in the Venturi system

Trials at air flow rates of 4, 5, and 6 L/min revealed that 5 L/min was the most optimal condition. At this flow rate, medium-sized bubbles were formed stably and rose uniformly, enhancing the particle–bubble contact efficiency. In contrast, the 4 L/min flow produced small but unstable bubbles, whereas the 6 L/min flow generated larger bubbles that were less stable and less uniformly distributed (Table 5). Figure 3 shows the bubble formation in the Venturi system at different air flows.

Table 5 Effect of air flow rate on bubble formation characteristics

Air flow (L/min)	Retention time (s)	Bubble Size	Bubble Stability
4	42	Small	Not rising, unstable
5	34	Medium	Rising, stable
6	20	Large	Rising, unstable

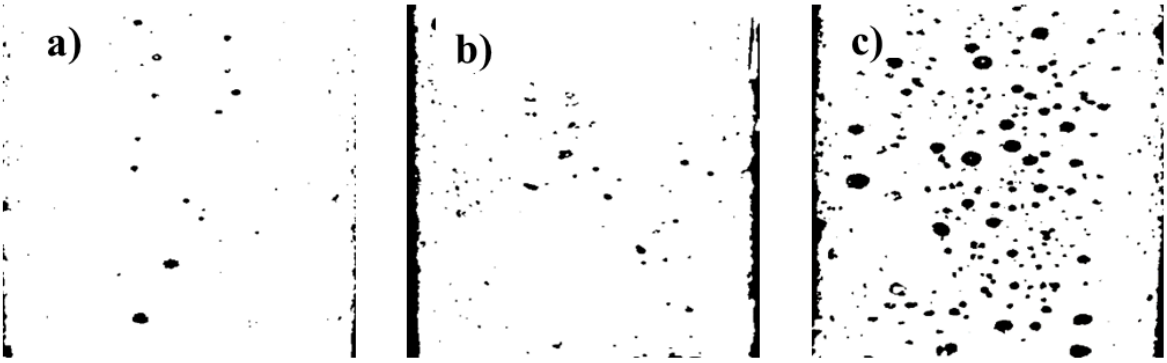

Figure 3 Bubble formation in the Venturi system at airflow rates of (a) 4, (b) 5, and (c) 6 L/min

3.1.2 Flotation Experiments

At pH 4 (Figure 4a), the flotation recovery of galena remained relatively high across all starch concentrations, decreasing only slightly from 77.09% to 68.27%. This indicates that galena floatability is well maintained even with increasing corn starch dosage under acidic conditions. However, sphalerite recovery declined more noticeably from 52.46% at 0 ppm to 41.32% at 25 ppm, indicating moderate depression. The most significant suppression was observed in pyrite, where recovery dropped from 40.37% to 33.58%, implying a strong interaction between the depressant and Fe-sulfide surfaces. This result confirms that acidic pH enhances the selective depression of pyrite, with corn starch showing preferential adsorption onto its surface, potentially due to favorable electrostatic or chemical interactions (Mu et al., 2015; Chimonyo et al., 2020).

At neutral pH (Figure 4b), the selectivity effect of corn starch was less pronounced. Galena recovery remained relatively constant, ranging from 70.77% to 72.69%, whereas Zn and Fe recovery exhibited minor variations: Zn recovery ranged from 36.15% to 37.10%, and Fe recovery ranged from 30.90% to 32.86%. This trend suggests that corn starch adsorption onto mineral surfaces is reduced at pH 7, possibly due to a lower availability of hydroxyl species on sulfide surfaces that promote binding (Chen, 2021; Protopopoff & Marcus, 2003). The decreased differentiation in flotation behavior across the three minerals indicates weakened selectivity at neutral conditions, limiting the depressant's effectiveness for targeted separation.

Under alkaline conditions, selective depression was reestablished (Figure 4c). Galena continued to float efficiently, with recovery values decreasing only slightly from 77.74% to 73.45%. In contrast, sphalerite recovery decreased from 42.42% to 37.77%, and pyrite showed the most notable reduction, with recovery dropping from 34.65% to 30.97%. The results confirm that corn starch is more effective as a pyrite depressant at high pH, likely due to increased Fe-hydroxide species formation on the pyrite surface (Yang et al., 2021; Murphy and Strongin, 2009). These hydroxide layers facilitate polysaccharide adsorption, enhancing hydrophilicity and reducing flotation. The moderate depression of Zn suggests some degree of non-selective adsorption, yet the high Pb recovery demonstrates that selective flotation remains feasible under these conditions (Khoso et al., 2021; Mkhonto et al., 2024).

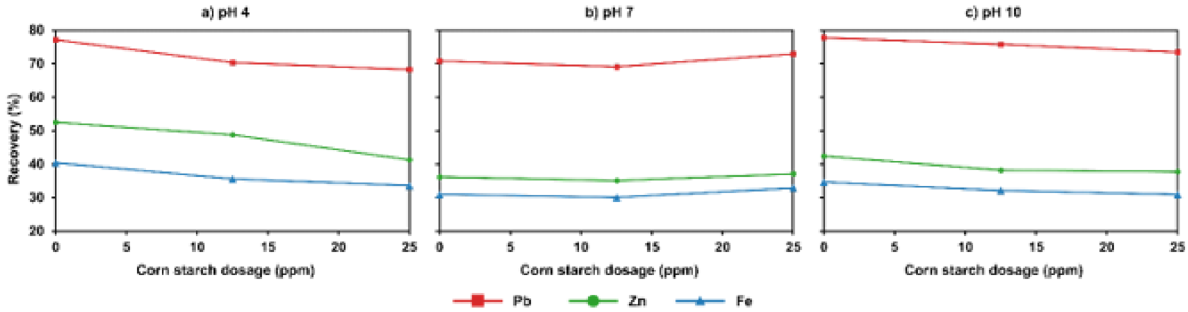

Figure 4 Effect of corn starch dosage on Pb, Zn, and Fe recovery at different pH conditions: (a) 4, (b) 7, and (c) 10

The flotation recovery gap between the target minerals (Pb and Zn) and the gangue mineral (Fe) serves as a key indicator of the selective separation effectiveness. A greater gap reflects better depressant selectivity, where the desired mineral remains floatable and the gangue is suppressed. The Pb–Fe recovery gap exhibited distinct trends across different pH levels and corn starch concentrations (Figure 5a). At pH 4, the gap decreased from 36.73% at 0 ppm to 34.69% at 25 ppm, indicating that while galena floatability remained high, the selectivity slightly declined with increased starch dosage due to mild co-depression. At pH 7, the gap remained relatively stable between 39.87% and 39.83%, indicating minimal interaction and selectivity between Pb and Fe under neutral conditions. Conversely, a pH of 10 resulted in the most favorable separation, with the Pb–Fe gap reaching a maximum of 43.62% at 12.5 ppm, signifying that alkaline conditions enhance starch adsorption onto pyrite while maintaining galena flotation. This confirms that a pH of 10 and moderate starch concentration provide optimal conditions for selective Pb–Fe separation (Yang et al., 2021; Murphy and Strongin, 2009).

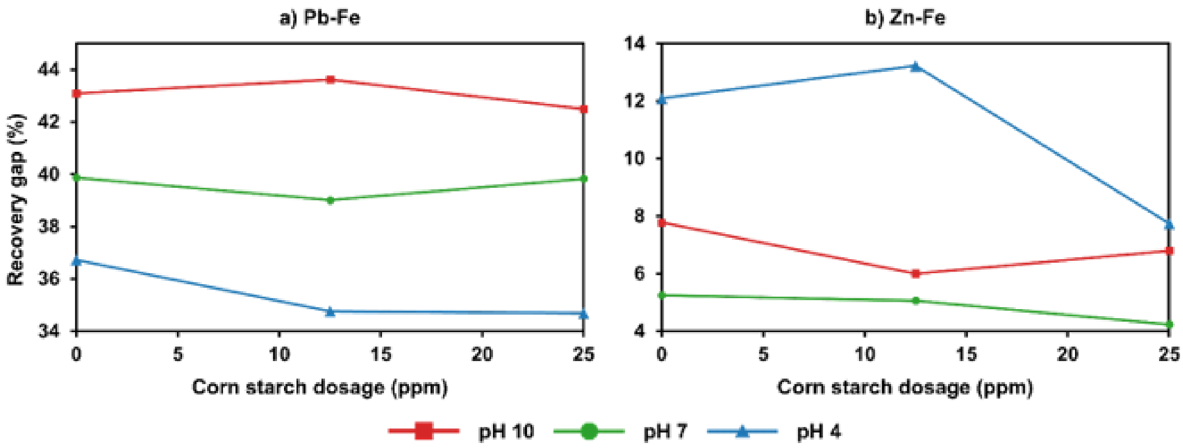

(a)

Figure 5 Recovery gap between (a) Pb–Fe and (b) Zn–Fe as a function of corn starch dosage at different pH values

Figure 5b illustrates the Zn–Fe recovery gap under similar conditions. At pH 4, the gap initially increased from 12.09% to 13.22% at 12.5 ppm, indicating improved selectivity, but then sharply decreased to 7.74% at 25 ppm due to significant sphalerite depression at higher starch concentrations. At pH 7, the recovery gap gradually declined from 5.25% to 4.24%, reflecting the ineffective selective behavior of corn starch between Zn and Fe under neutral pH. In contrast, pH 10 showed a slight fluctuation in the recovery gap from 7.78% to 6.00% and back to 6.80%, indicating moderate but unstable selectivity. The Zn–Fe recovery gaps were consistently smaller and more sensitive to both pH and starch dosage than the Pb–Fe separation, showing a weaker discrimination by the depressant between sphalerite and pyrite. Collectively, these findings show that corn starch has the highest selectivity for Pb–Fe separation under alkaline conditions, while its application for Zn–Fe separation is limited and requires tighter control of flotation parameters to avoid non-selective depression.

As shown in Figures 6a (pH 4) and 6b (pH 10), the intensity and distribution of the diffraction peaks reflect the mineral composition in the concentrate and tailing phases. At pH 4, sphalerite (ZnS) peaks are prominently present in the concentrate, while pyrite (FeS_2) signals remain stronger in the tailing, indicating that pyrite contamination is minimal and sphalerite recovery is effective. Conversely, at pH 10, the peaks corresponding to galena (PbS) are clearly enriched in the concentrate phase, whereas pyrite remains predominantly in the tailings. At 12.5 ppm, corn starch inhibited pyrite flotation while retaining galena and sphalerite hydrophobicity, indicating improved separation with pH and starch.

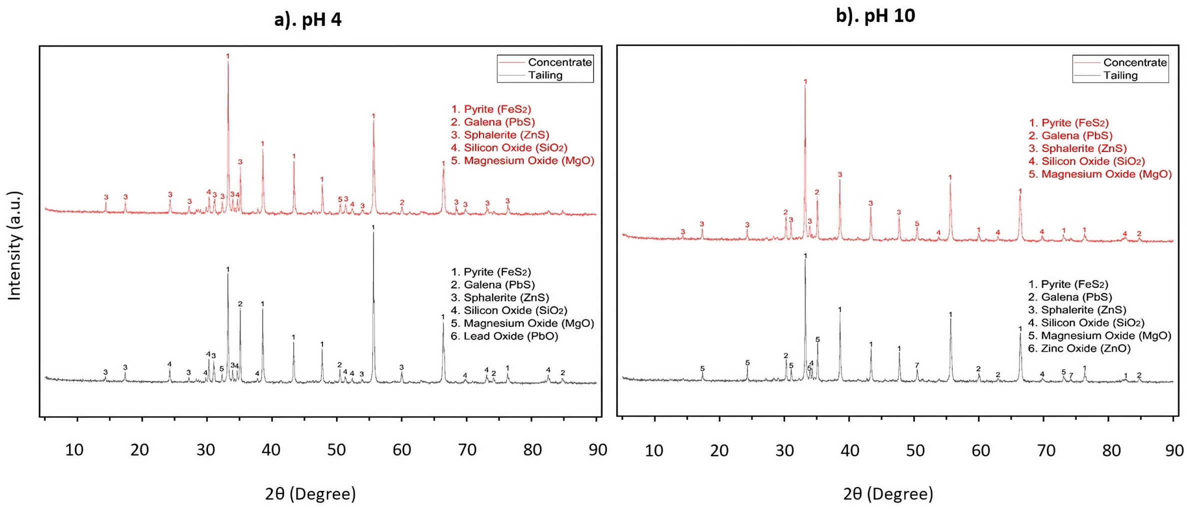

Figure 6 X-ray diffraction characterization of flotation concentrate and tailing at (a) pH 4 and (b) pH 10

Based on the Pourbaix diagrams of Pb, Zn, and Fe in Figure 7, the surface chemistry strongly influences selective flotation. At pH 4, both galena and pyrite are electrochemically active, resulting in poor selectivity. As the pH increases to 7, pyrite begins to form hydrophilic oxide/hydroxide layers, while galena remains partially floatable. At pH 10, galena forms PbO but still exhibits flotation activity, whereas pyrite is strongly passivated as Fe_2O_3/Fe_3O_4, reducing its hydrophobicity. Similarly, sphalerite (ZnS) shows favorable flotation at low pH, with Zn remaining active, while higher pH induces $Zn(OH)_2$ formation, lowering its floatability. Therefore, high pH favors galena–pyrite separation, whereas low pH enhances sphalerite recovery over pyrite.

3.2 Discussion

The findings of this study clearly show that integrating a Venturi-type flotation column with corn starch as a biodegradable depressant significantly improves the selective separation of galena (Pb) and sphalerite (Zn) from pyrite (Fe) under controlled pH conditions. The interaction between pH and starch dosage strongly governs the selectivity mechanism, as demonstrated by individual recovery values and recovery gaps. At pH 4, the highest recovery for Pb (77.09%) was recorded in the absence of corn starch, while the recovery for Fe reached 40.37%. As the starch dosage was increased to 25 ppm, the Pb recovery decreased to 68.27% and the Fe recovery to

33.58%, indicating the effectiveness of corn starch in depressing pyrite while preserving the moderate flotation performance for Pb. However, Zn was more affected by starch addition, dropping from 52.46% to 41.32%. This trend confirms that corn starch is more selective toward depressing Fe than Pb or Zn, with the strongest selectivity observed for Pb–Fe separation. These results are consistent with those of prior studies showing that polysaccharides such as dextrin and carboxymethyl cellulose (CMC) selectively depress pyrite through surface adsorption, particularly under acidic to neutral conditions (Ahmadi et al., 2018; Khoso et al., 2021).

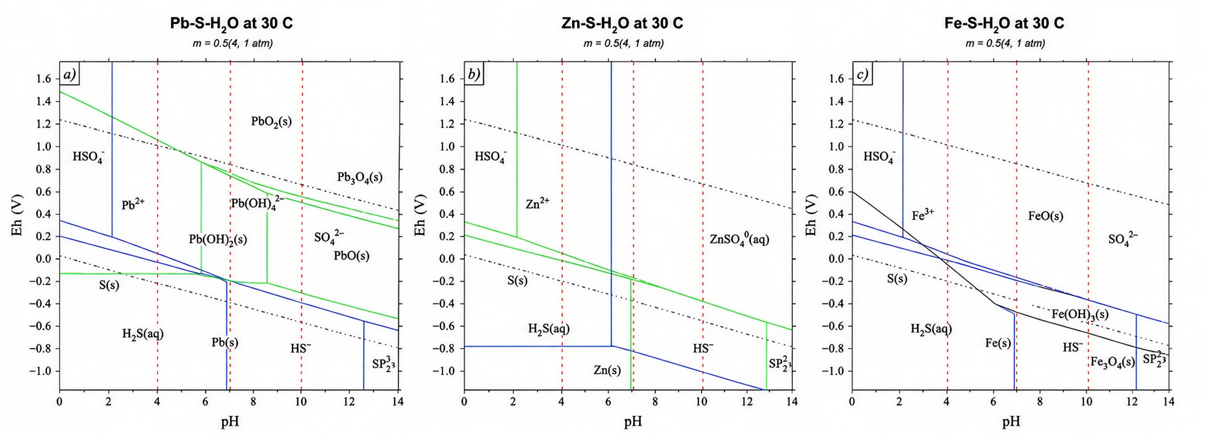

Figure 7 Pourbaix diagrams of the stability regions of the (a) Pb–H_2O, (b) Zn–H_2O, and (c) Fe–H_2O systems

At pH 7, the effect of corn starch was less pronounced. The Pb recovery remained relatively stable across all concentrations, from 70.77% to 72.69%, whereas the Fe recovery slightly increased from 30.90% to 32.86%. The Zn recovery trend showed a slight increase from 36.15% to 37.10% at 25 ppm. This demonstrates that near-neutral pH may reduce the surface activity of starch molecules, thereby weakening their selective adsorption on mineral surfaces (Wang & Liu, 2021). Consequently, selectivity in this condition was moderate, as supported by the Pb–Fe and Zn–Fe gap data. Corn starch continued to depress Fe more significantly than Pb or Zn at pH 10. The Pb recovery remained high (77.74% → 73.45%), while the Fe recovery dropped from 34.65% to 30.97%. Notably, Zn recovery also decreased from 42.42% to 37.77%. This supports the hypothesis that the formation of hydroxylated species on pyrite surfaces under alkaline conditions enhances starch adsorption via electrostatic and acid–base interactions (Han et al., 2019; Ran et al., 2023; Zhai et al., 2024). However, Zn is also partly suppressed at high starch concentrations, likely due to non-selective surface interactions or changes in zeta potential (Wei et al., 2024; Chandra and Gerson, 2009). The GRPs confirm the selectivity trends. The Pb–Fe recovery gap peaked at 43.62% (pH 10, 12.5 ppm), while the Zn–Fe gap peaked at 13.22% (pH 4, 12.5 ppm), indicating that the separation of Pb from Fe is more effective than that of Zn from Fe in this system. The relatively lower Zn–Fe gap indicates weaker selectivity, possibly due to similar surface chemistry or less effective depression of pyrite at lower Zn pH.

The air flow rate strongly influences the performance of the Venturi-type bubble generator, which governs gas dispersion, bubble formation, and particle–bubble collision efficiency. As shown in Table 3, increasing the air flow rate from 4 to 6 L/min produced notable changes in bubble size, retention time, and bubble stability. At 4 L/min, the system generated small bubbles with the longest retention time (42 s). However, the bubbles were unstable and did not rise efficiently, likely due to insufficient kinetic energy for vertical transport in the column.

Although fine bubbles are typically favorable for flotation, mineral attachment and recovery may be hindered by instability and poor ascent behavior. The retention time decreased to 34 s at 5 L/min, and medium-sized bubbles were formed with good stability and upward motion, indicating an optimal balance between bubble dispersion and lift. This condition enhanced the probability of effective particle–bubble collision and attachment, particularly for hydrophobic minerals such as galena and sphalerite, while minimizing the entrainment of hydrophilic pyrite. These observations correlate with the maximum Pb–Fe selectivity achieved at this flow rate and pH of 10, reinforcing the hypothesis that controlled turbulence and stable bubbles are critical for flotation performance.

At 6 L/min, although the bubbles rose quickly, they were larger and less stable, with a shorter retention time (20 s). This resulted in more turbulent mixing and decreased selectivity due to the increased entrainment of fine gangue particles, such as pyrite. Larger bubbles also tend to have lower surface area-to-volume ratios, reducing the particle collection efficiency. These findings are consistent with those who noted that excess air flow may compromise selectivity despite increasing flotation kinetics (Peleka et al., 2017; Wang and Liu, 2021). The Venturi throat velocity profile complements these observations. The highest air velocity was recorded at 6 L/min at the throat, indicating intense shearing conducive to bubble formation. However, the maximum air velocity does not always correlate with optimal flotation, particularly if bubble stability is compromised. The moderate air velocity at 5 L/min provided a more stable hydrodynamic regime, promoting selective flotation while maintaining energy efficiency. Therefore, this study highlights the importance of optimizing the air flow rate in Venturi-based systems to balance the bubble size, stability, and retention time. This approach enables efficient flotation of target minerals while suppressing gangue, further strengthening the role of Venturi column flotation as a low-energy, high-selectivity alternative to conventional flotation cells.

However, this study was limited to synthetic minerals under batch laboratory conditions, and the interaction mechanisms were not directly measured using FTIR or zeta potential. Future research should include (1) testing on natural polymetallic ores, (2) conducting adsorption mechanism studies, (3) exploring alternative biopolymer blends, and (4) scaling up to continuous pilot or industrial-scale Venturi flotation.

4. Conclusions

This study demonstrates that using a Venturi flotation column along with eco-friendly corn starch depressants can enhance the separation of galena and sphalerite from pyrite. Changing the pH level and the amount of depressant used significantly influences the effectiveness of the flotation process. When the pH is carefully controlled and the right depressants are used, column froth flotation helps recover more lead from galena. In this study, the suitable parameter was set at an air flow rate of 5 L/min, producing steady and properly sized bubbles that enhanced the flotation process. The highest separation result in this study was achieved at a pH of 10 for galena and a pH of 4 for sphalerite, with 12.5 ppm of corn starch effectively reducing the floating of pyrite.

Acknowledgements

Hibah PUTI Q2 with contract number: NKB-1733/UN2.RST/HKP.05.00/2020.

Conflict of Interest

The authors declare no conflicts of interest.

References

Ahmadi, M., Gharabaghi, M., & Abdollahi, H. (2018). Effects of type and dosages of organic depressants on pyrite floatability in microflotation system. *Advanced Powder Technology*, *29*(12), 3155–3162. https://doi.org/10.1016/j.apt.2018.08.015

Asimi-Neisiani, A., Saneie, R., Mohammadzadeh, A., Wonyen, D. G., & Chehreh Chelgani, S. (2023). Polysaccharides-based pyrite depressants for green flotation separation: An overview. *International Journal of Mining Science and Technology*, *33*(10), 1229–1241. https://doi.org/10.1016/j.ijmst.2023.09.002

Chandra, A. P., & Gerson, A. R. (2009). A review of the fundamental studies of the copper activation mechanisms for selective flotation of the sulfide minerals, sphalerite and pyrite. *Advances in Colloid and Interface Science*, *145*(1–2), 97–110. https://doi.org/10.1016/j.cis.2008.09.001

Chen, J. (2021). The interaction of flotation reagents with metal ions in mineral surfaces: A perspective from coordination chemistry. *Minerals Engineering*, *171*. https://doi.org/10.1016/j.mineng.2021.107067

Chimonyo, W., Fletcher, B., & Peng, Y. (2020). Starch chemical modification for selective flotation of copper sulphide minerals from carbonaceous material: A critical review. *Minerals Engineering*, *156*. https://doi.org/10.1016/j.mineng.2020.106522

Han, G., Wen, S., Wang, H., & Feng, Q. (2019). Effect of starch on surface properties of pyrite and chalcopyrite and its response to flotation separation at low alkalinity. *Minerals Engineering*, *143*. https://doi.org/10.1016/j.mineng.2019.106015

Khoso, S. A., Hu, Y., Tian, M., Gao, Z., & Sun, W. (2021). Evaluation of green synthetic depressants for sulfide flotation: Synthesis, characterization and floatation performance to pyrite and chalcopyrite. *Separation and Purification Technology*, *259*. https://doi.org/10.1016/j.seppur.2020.118138

Li, M. (2022). Fundamental understanding on the inception of hydrodynamic cavitation and its generated microbubbles in fine particle flotation.

Li, M., Bussionère, A., Bronson, M., Xu, Z., & Liu, Q. (2018). Study of Venturi tube geometry on the hydrodynamic cavitation for the generation of microbubbles [(in press)]. *Minerals Engineering*.

Mkhonto, P. P., Zhang, X., McFadzean, B., Taguta, J., Zhu, Y., Han, L., & Ngoepe, P. E. (2024). Incorporating pH into DFT-D+U and microflotation recovery studies on heterocyclic collector-pyrite interactions. *Separation and Purification Technology*, *337*. https://doi.org/10.1016/j.seppur.2024.126430

Mu, Y., Peng, Y., & Lauten, R. A. (2015). Electrochemistry aspects of pyrite in the presence of potassium amyl xanthate and a lignosulfonate-based biopolymer depressant. *Electrochimica Acta*, *174*(1), 133–142. https://doi.org/10.1016/j.electacta.2015.05.150

Mu, Y., Peng, Y., & Lauten, R. A. (2016). The depression of pyrite in selective flotation by different reagent systems—A literature review. *Minerals Engineering*, *96–97*, 143–156. https://doi.org/10.1016/j.mineng.2016.06.018

Murphy, R., & Strongin, D. R. (2009). Surface reactivity of pyrite and related sulfides. *Surface Science Reports*, *64*(1), 1–45. https://doi.org/10.1016/j.surfrep.2008.09.002

Nagaraj, D. R., & Farinato, R. S. (2016). Evolution of flotation chemistry and chemicals: A century of innovations and the lingering challenges. *Minerals Engineering*, *96–97*, 2–14. https://doi.org/10.1016/j.mineng.2016.06.019

Nayak, A., Jena, M. S., & Mandre, N. R. (2022). Beneficiation of Lead-Zinc ores—a review. *Mineral Processing and Extractive Metallurgy Review*, *43*(5), 564–583. https://doi.org/10.1080/08827508.2021.1903459

Peleka, E. N., Gallios, G. P., & Matis, K. A. (2017). A perspective on flotation: A review. *Journal of Chemical Technology and Biotechnology*, *93*(3), 615–623.

Prameswara, G., Trisnawati, I., Handini, T., Poernomo, H., Mulyono, P., Prasetya, A., & Petrus, H. T. M. B. (2023). Recovery of critical elements (dysprosium and ytterbium) from alkaline process of indonesian zircon tailings: Selective leaching and kinetics study. *International Journal of Technology*, *14*(4), 770–779. https://doi.org/10.14716/ijtech.v14i4.4960

Prasad, M. S. (1992). Reagents in mineral technology. *Minerals Engineering*, *5*(3–5), 279–294. https://doi.org/10.1016/0892-6875(92)90211-Q

Protopopoff, E., & Marcus, P. (2003). Potential-pH diagrams for sulfur and hydroxyl adsorbed on copper surfaces in water containing sulfides, sulfites or thiosulfates [(in press)]. *Corrosion Science*. www.elsevier.com/locate/corsci

Qin, W., Wei, Q., Jiao, F., Yang, C., Liu, R., Wang, P., & Ke, L. (2013). Utilization of polysaccharides as depressants for the flotation separation of copper/lead concentrate. *International Journal of Mining Science and Technology*, *23*(2), 179–186. https://doi.org/10.1016/j.ijmst.2013.04.022

Ran, J., Li, Y., Zhao, X., Jiang, M., & Gao, E. (2023). Utilization of soluble starch as the depressant to flotation separation of pyrite from arsenopyrite. *Separation and Purification Technology*, *310*. https://doi.org/10.1016/j.seppur.2023.123155

Sakamatapan, K., Mesgarpour, M., Mahian, O., Ahn, H. S., & Wongwises, S. (2021). Experimental investigation of the microbubble generation using a venturi-type bubble generator. *Case Studies in Thermal Engineering*, *27*. https://doi.org/10.1016/j.csite.2021.101238

Tjhia, M. A., Yahya, M. N. F., & Ulum, R. M. (2024). Characteristics of treated monazite in different particle sizes to upgrade the rare earth elements content by using mechanochemical and roasting processes. *International Journal of Technology*, *15*(2), 463–471.

Trisnawati, I., Prameswara, G., Mulyono, P., Prasetya, A., & Petrus, H. T. B. M. (2020). Sulfuric acid leaching of heavy rare earth elements (HREEs) from indonesian zircon tailing. *International Journal of Technology*, *11*(4), 804–816. https://doi.org/10.14716/ijtech.v11i4.4037

Wang, D., & Liu, Q. (2021). Hydrodynamics of froth flotation and its effects on fine and ultrafine mineral particle flotation: A literature review. *Minerals Engineering*, *173*. https://doi.org/10.1016/j.mineng.2021.107220

Wang, Y. (2002). Preparation of nanocrystalline metal oxide powders with the surfactant-mediated method. *Inorganic Chemistry Communications*, *5*, 751–755.

Wei, B., Mao, Y., Wang, L., Shen, P., Wang, H., & Liu, D. (2024). Sources, performance and mechanisms of metal ions in the flotation process of copper, lead, and zinc ores: A review. *Minerals*, *14*(11). https://doi.org/10.3390/min14111105

Wills, B. A., & Finch, J. A. (2016). *Wills' mineral processing technology: An introduction to the practical aspects of ore treatment and mineral recovery* (8th ed.). Elsevier Science; Technology Books.

Xiong, Y., & Peng, F. (2015). Optimization of cavitation venturi tube design for pico and nano bubbles generation. *International Journal of Mining Science and Technology*, *25*(4), 523–529. https://doi.org/10.1016/j.ijmst.2015.05.002

Yang, B., Zhu, H., Zeng, L., Feng, J., & Luo, H. (2021). An environmental-friendly sphalerite depressant (2-hydroxyphosphonoacetic acid) for the selective flotation separation of sphalerite from galena. *Journal of Molecular Liquids*, *343*. https://doi.org/10.1016/j.molliq.2021.117614

Zhai, Q., Hu, Y., Liu, R., & Sun, W. (2024). Investigation of pullulan polysaccharide as a sphalerite depressant for chalcopyrite separation: Flotation behavior and interfacial adsorption mechanism. *Advanced Powder Technology*, *35*(10). https://doi.org/10.1016/j.apt.2024.104621

Zhao, L., Li, K., Matkarimov, S. T., Liu, C., Bao, S., & Yang, S. (2025). Mechanical activation improves green depressant starch for the flotation separation of pyrite from chalcopyrite via molecular structure optimization. *Journal of Molecular Liquids*, *424*. https://doi.org/10.1016/j.molliq.2025.127122

Zhou, S., Wang, X., Bu, X., Wang, M., An, B., Shao, H., Ni, C., Peng, Y., & Xie, G. (2020). A novel flotation technique combining carrier flotation and cavitation bubbles to enhance separation efficiency of ultra-fine particles. *Ultrasonics Sonochemistry*, *64*. https://doi.org/10.1016/j.ultsonch.2020.105005

Zhou, Y., Cui, J., Chen, Z., Liu, J., He, L., Fan, W., & Huo, M. (2025). Parametric analysis of venturi-type microbubble generator and the bubble fragmentation dynamics. *Desalination and Water Treatment*, *322*. https://doi.org/10.1016/j.dwt.2025.101116